Coupling CP-MD Simulations and X-ray Absorption Spectroscopy: Exploring the Structure of Oxaliplatin in Aqueous Solution

Elizabeth C. Beret,[†] Karine Provost,[‡] Diane Müller,[‡] and Enrique Sánchez Marcos*[,†]

Departamento de Química Física, Universidad de Sevilla, 41012 Sevilla, Spain, and Institut de Chimie et des Matériaux Paris Est, ICMPE/SAX, UMR 7182 CNRS, Université Paris 12, PRES Paris Est, 94320 Thiais, France

Received: June 09, 2009; Revised Manuscript Received: July 21, 2009

A combined experimental−theoretical approach applying X-ray absorption spectroscopy and ab initio molecular dynamics (CP-MD) simulations is used to get insight into the structural determination of oxaliplatin, a third-generation anticancer drug of the cisplatin family, in aqueous solution. Experimental Pt L_{III}-edge EXAFS and XANES spectra of oxaliplatin in water are compared with theoretical XAS spectra. The latter are obtained as statistically averaged spectra computed for a set of selected snapshots extracted from the MD trajectory of ethyldiamineoxalatoplatinum(II) (EDO−Pt) in liquid water. This compound is a simplified structure of oxaliplatin, where the outer part of the cyclohexane ring contained in the cyclohexanediamine ligand of oxaliplatin has been removed. We show that EDO−Pt is an appropriate model to simulate the spectroscopical properties of oxaliplatin given that the cyclohexane ring does not generate particular features in neither the EXAFS nor the XANES spectra. The computation of average EXAFS spectra using structures from the MD simulation in which atoms are selected according to different cutoff radii around the Pt center allows the assignment of spectral features to particular structural motifs, both in k and R-spaces. The outer oxygen atoms of the oxalate ligand ($R_{Pt-O_{II}} = 3.97 \pm 0.03$ Å) are responsible for a well-defined hump at around 6.5 $Å^{-1}$ in the k^2-weighted EXAFS spectrum. The conventional EXAFS analysis data procedure is reexamined by its application to the simulated average EXAFS spectra. The structural parameters resulting from the fit may then be compared with those obtained from the simulation, providing an estimation of the methodological error associated with the global fitting procedure. A thorough discussion on the synergy between the experimental and theoretical XAS approaches is presented, and evidence for the detection of a slight hydration structure around the Pt complex is shown, leading to the suggestion of a new challenge to experimental XAS measurements.

1. Introduction

Oxaliplatin {*cis*-[(1*R*,2*R*)-1,2-cyclohexanediamine-*N*,*N*′]-oxalatoplatinum(II)} is a third-generation anticancer drug of the cisplatin [*cis*-$Pt(NH_3)_2Cl_2$] family that was approved for the treatment of colorectal cancer in the European Union in 1999 and in the United States in 2002.[1] Since the discovery of these drugs the healing and global survival rates in patients suffering this type of disease have raised remarkably.[2,3] The global action mechanism of this drug is not completely understood, in part due to the fact that its marked antitumor efficacy is currently obtained by its combination with other chemical compounds.[4] However, at a biochemical level it is generally accepted that cisplatin compounds form Pt−DNA adducts inside the cellular nucleus that suppress protein synthesis, leading to a preferential death of cancer cells.[5,6] In this scenario, one important step in the effort to understand the global mechanism is the structural characterization of oxaliplatin in solution. In a recent study concerning chelating ligands closely related to those present in the anticancer derivatives of cisplatin, Peacock et al.[7] have underlined that the potential biological and medical applications of organometallic complexes are hampered by a lack of knowledge of their behavior in the aqueous environment.

The implicitly low concentration of oxaliplatin in solution forces the use of X-ray absorption spectroscopy as the most suitable technique to supply direct structural information on the system. In particular, extended X-ray absorption fine structure (EXAFS) has already been employed by some of us to undertake the analysis of solid and liquid samples of oxaliplatin.[8,9] From these studies the values of the Pt−O and Pt−N distances in the first coordination shell and the Pt−C and Pt−O distances within the second shell were obtained on the basis of simplified assumptions concerning the Debye−Waller factors associated with both the single and multiple scattering paths. It must be stressed that the structural planarity and rigidity of oxaliplatin lead to involved contributions from a large number of scattering paths to the EXAFS function.

The strategy of reducing the degree of uncertainty in the analysis of EXAFS spectra by including independent microscopic information derived from computer simulations has been proved useful during the last years for metal ions in solution.[10−14] An additional step in this direction has been the extension of a similar coupling between theoretical and experimental techniques to the analysis of the XANES part of the spectrum.[14−16] In a very recent theoretical study,[17] a complete set of molecular dynamics (MD) trajectories of a model of oxaliplatin in liquid water was obtained by means of ab initio MD simulations within the Car−Parrinello MD (CP-MD) formalism.[18,19]

* To whom correspondence should be addressed. E-mail: sanchez@us.es.
† Universidad de Sevilla.
‡ Université Paris 12.

10.1021/jp905415v CCC: $40.75
Published on Web 08/17/2009

The aim of the present study is to explore the detection limits and capabilities of the XAS techniques in the structural elucidation of oxaliplatin in liquid water, which is achieved by coupling the experimental information contained in the EXAFS and XANES spectra with the structural and dynamic microscopical description provided by the CP-MD statistical trajectories. We present novel studies concerning the XANES part of the spectrum, the effect of the solvent on the XAS properties of oxaliplatin, and the assignment of features in the EXAFS spectrum to structural motifs, both in *k*- and *R*-spaces. The synergy between XAS techniques and MD simulations provides a refinement of the standard EXAFS analysis procedure when such an analysis is applied on theoretical EXAFS spectra obtained from the MD trajectory, as already proposed in previous studies of Cr(III), Rh(III), and Ir(III) metal ions in bulk water.[13,14,20] The comparison of the structural data extracted from the EXAFS analysis with those derived from the CP-MD simulations sheds light on the number of coordination shells around Pt(II) that may be detected and on the accuracy of the geometrical parameters extracted. Finally, the methodology developed in this paper aims to help the further determination of products derived from the physiological degradation of oxaliplatin in biological media, which takes place during the therapeutic activity of the drug.

2. Methods

2.1. Theoretical Spectra. Theoretical EXAFS and XANES spectra of the L_{III}-edge of Pt in oxaliplatin have been computed using a statistically meaningful high number of snapshots extracted from the CP-MD simulation of ethyldiamineoxalatoplatinum(II) (EDO−Pt) in aqueous solution described in ref 17. EDO−Pt is a simplified structure obtained from oxaliplatin by removing the outer part of the cyclohexane ring (see Figure 1).

The individual XAS spectra $\chi_M(k)$ obtained for each snapshot *M* are later averaged to yield a global XANES or EXAFS spectrum $\chi(k)$:

$$\overline{\chi(k)} = \frac{1}{N_{\mathrm{MD}}} \sum_{M}^{N_{\mathrm{MD}}} \chi_M(k) \qquad (1)$$

In the case of the EXAFS spectrum, the average signal can be described using the following mathematical formulation:[13]

$$\overline{\chi}(k) = \frac{1}{N_{MD}} \sum_{M}^{N_{MD}} \sum_{i}^{paths} \frac{N_i S_0^2 \left| f^{eff}(k,R) \right|_i}{kR_{Mi}^2} e^{-2R_{Mi}/\lambda} \sin(2kR_{Mi} + \alpha_{Mi}(k)) \qquad (2)$$

where the *M* index runs over the N_{MD} considered snapshots and *i* index refers to a given scattering path. Here the thermal and structural disorder is not represented by a Debye−Waller factor, but it arises from summing over a high number of MD structural arrangements. In this contribution we have used a series of 250 snapshots extracted from the CP-MD simulation of EDO−Pt in water. The use of a higher number of snapshots (500) did not introduce any observable changes into the spectrum, and therefore, the selected series of 250 structures is enough to yield a statistically meaningful representation of the system.

In addition, EXAFS and XANES spectra have been computed for the gas-phase optimized structures of oxaliplatin and EDO−Pt. These structures were obtained by means of quantum-mechanical geometry optimizations using the PBE exchange and correlation functional,[21] with energy-consistent pseudopotentials from the Stuttgart/Köln group and their corresponding optimized valence basis sets for Pt[22] and aug-cc-pVDZ basis sets for the rest of atoms.[23]

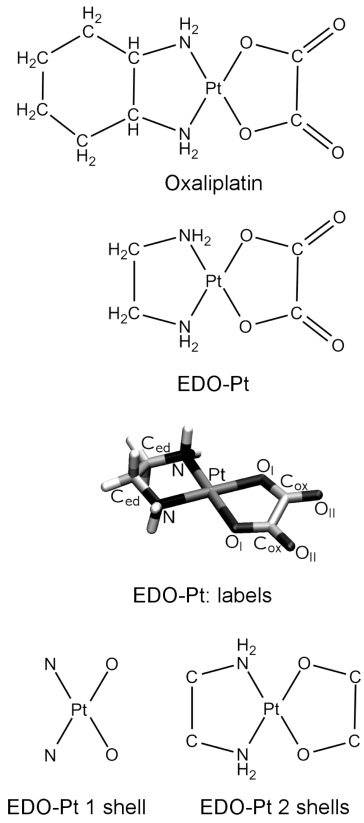

Figure 1. From top to bottom: Chemical structures of oxaliplatin, its molecular model EDO−Pt and atom labels used within the article, and the other two reduced structural units considered in the calculation of simulated EXAFS spectra.

XAS calculations were performed with the FEFF8 code.[24,25] For both EXAFS and XANES simulated spectra, the Hedin−Lundqvist exchange-correlation potential was used to compute the electron density distribution within a self-consistent-field approach.[24,26] The chemical differences between oxygen atoms belonging to the oxalate ligand and those of water molecules were considered by means of computation of distinct backscattering potentials. Hydrogen atoms were taken into account to compute the potential during the SCF procedure, but they were not included as backscatterers. In the case of XANES spectra, full multiple scattering computations were performed within a sphere of appropriate radius (6 Å) around the Pt center, and the Fermi level was shifted 7 eV. In the case of EXAFS spectra, the only parameter not derived from computations was the amplitude reduction function, S_0^2, that was set up to 0.94 in order to match the first peak height in the Fourier transforms (FT) of the experimental and simulated EXAFS spectra. A similar strategy to obtain simulated EXAFS and XANES spectra of different ions in solution has already been applied in previous works.[13−15,20,27,28]

2.2. Experimental Spectra. Powdered oxaliplatin was obtained from a Sanofi pharmaceutical preparation. Solid samples were prepared as a homogeneous mixture of oxaliplatin powder and cellulose compressed pellets. The quantity of product was calculated in order to obtain an edge jump $\Delta\mu x$ near 1, with a total absorbance after the edge $\Delta\mu x(E) < 2$. For the solution samples, the powder was diluted to 10 mg/mL (25 mM) in pure water. Oxaliplatin solid and liquid XAS spectra were recorded

in transmission mode, respectively, at LURE (Orsay, France, EXAFS13 station of the DCI storage ring) for the solid sample and ELETTRA (Trieste, Italy, BL11.1 station) for the liquid sample, at the Pt L_{III}-edge. For the solid sample we used a Si(111) channel-cut monochromator, together with an energy range of 11 450−12 600 eV. For the liquid sample, the experimental conditions were Si(111) double crystal monochromator, with an energy range of 11 260−13 000 eV.

The spectra were extracted using standard procedures[29−31] available in the program Cherokee,[32] including spline smoothing atomic absorption determination, energy-dependent normalization, and fast Fourier transform (E_0 taken at the inflection point, FT range 2.36−16 Å^{-1}). Each spectrum was recorded three times in order to estimate the average and the experimental errors.

2.3. EXAFS Fitting Procedure. For both theoretical and experimental spectra, EXAFS data analysis was performed under the same conditions and included the following steps:

i Ab-initio EXAFS calculation was done with FEFF8[24,25] on the basis of the crystallographic structure without any hydrogen atoms.[33] FEFF8 input files were prepared with the code CRYSTALFF.[34] As the E_0 energy is fitted, no self-consistent field was included in the calculation of the potentials.

ii The most important single and multiple scattering paths up to 5 Å were sorted with the use of the homemade software Amplitude. Above this limit, the EXAFS signal appears to be negligible. This leads to a seven-shell model including single scattering by the first neighbors (four Pt−N/O paths), single scattering by the carbon atoms of oxalate and diamine cyclohexane (two Pt−C_{ox}, two Pt−C_{ed} paths), single and multiple scattering characteristic of the oxalate (two Pt−O_{II}, four Pt−C−O_{II}, two Pt−C−O_{II}−C paths), and multiple scattering through the platinum atom (four Pt−N−Pt−O paths); see Figure 1 for atom labels.

iii The parameters of the different shells were fit by comparing the experimental spectra to the standard EXAFS formula[31] using the RoundMidnight code.[32] Due to the high correlation among different parameters, we introduced some constraints to the fits: The energy threshold was determined from a model including only single scattering by the first neighbors and was fixed to this value for the complete modeling. We applied a constant distance shift of 0.1 Å between the Pt−C_{ox} and Pt−C_{ed} signals (the corresponding distances in the crystallographic structure are respectively 2.77 and 2.90 Å), as well as between scattering paths of the oxalate (mean distance of 4.00 Å) and multiple scattering through the platinum atom (4.07 Å). We fitted two Debye−Waller factors, one accounting for single scattering by the first neighbors (σ_1^2) and the other one (σ_2^2) for multiple scattering within the first coordination shell and all single and multiple scattering paths beyond it. In order to keep consistency with the previous examination of oxaliplatin EXAFS spectra,[9] the photoelectron mean free path was set to the empirical minimal curve,[29] with $\Gamma = 0.7$ and $\eta = 3$.

iv Statistical errors (ε_i) on the average spectra and error bars for the fitted parameters are evaluated as recommended by the IXS Standard and Criteria Subcommittee.[35] According to these recommendations, the goodness of the fit or quality factor is $QF = \Delta\chi_{min}^2/\nu$, where $\Delta\chi_{min}^2$ is the minimum value of the statistical $\Delta\chi^2$ and ν is the degree of freedom, $\nu = N_{ind} - N_{par}$. N_{ind} is the number of independent points and N_{par} is the total number of fitted parameters. Since we use a k^3 weighting, the statistical $\Delta\chi^2$ is calculated as proposed by Vlaic et al.:[36]

$$\Delta_{\chi_{stat(weighted)}} = \frac{N_{ind}}{N_{pt}} \sum_i \omega(k_i)[k\chi_{th}(k_i) - k\chi_{exp}(k_i)]^2 \quad (3)$$

where N_{pt} is the number of experimental points, χ_{th} and χ_{exp} are the fitted and experimental EXAFS function, and $\omega(k) = Ak^3$, with $A = [\sum_i k_i^{-3}/(\langle\varepsilon\rangle^2 N_{pt})]$. The mean experimental error $\langle\varepsilon\rangle$ is calculated on $k\chi_{exp}$ spectra by evaluating the point dispersion, corrected by the Student statistics as recommended by the IXS Standard and Criteria Subcommittee.[35] The EXAFS spectra were fitted in the range 2.36−16 Å^{-1} without any filtering. In this range, $\langle\varepsilon\rangle = 0.015$ for liquid spectra registered at ELETTRA and $\langle\varepsilon\rangle = 0.027$ for solid spectra registered at LURE, and the ratio signal/noise are respectively 6.4 and 3.9. For theoretical spectra, we used the same $\langle\varepsilon\rangle = 0.015$ value as for liquid ELETTRA.

3. Results

3.1. Test of the Structural Model for Oxaliplatin. Figure 2 shows the experimental EXAFS and XANES spectra recorded for the liquid and solid samples of oxaliplatin (referred to as liquid ELETTRA and solid LURE, respectively) along with three theoretical spectra computed for different structural representations of oxaliplatin (read below for more details).

The experimental XANES spectra show three main features besides the pronounced white line: a hump appearing 24 eV above the main resonance (A) and two peaks at around 48 eV (B) and 118 eV (C) above the white line, the first of them being more intense and defined than the second one. The principal aim of the experiment carried out at LURE was the extraction of the EXAFS part of the XAS spectra, and therefore, a rather wide energy interval between points was defined in the XANES region. This lower resolution in the solid LURE spectrum compared to the liquid ELETTRA one leads to a quenching of the white line in the first case. However, the other features in the spectrum appear remarkably similar for both the solid and liquid samples. The EXAFS function obtained from experiment is a rather complex spectrum that contains different significant contributions to the final $\chi(k)$ function. The main features in the spectrum have been labeled A−D. The solid and liquid samples of oxaliplatin provide similar EXAFS experimental spectra.

In a previous CP-MD simulation[17] of EDO−Pt in aqueous solution, we checked that EDO−Pt yields a good structural model for oxaliplatin. The use of EDO−Pt instead of the full oxaliplatin complex allows us to perform ab initio MD simulations of oxaliplatin in liquid water, which otherwise would have a very high computational cost. Nevertheless, it is necessary to test its ability to mimic the XAS spectroscopic behavior of oxaliplatin. Therefore, theoretical EXAFS and XANES spectra for three different structural representations of oxaliplatin have been computed: its crystallographic structure (obtained from the crystallographic database; hydrogen atoms were added geometrically)[33] plus two structures quantum mechanically optimized in the gas phase, oxaliplatin and EDO−Pt. The EXAFS and XANES spectra, calculated under the same conditions, are very similar for the three structural models.

The calculated XANES reproduce quite well the relative positions of the white line and the three features in the experimental spectra. The intensity of the white line in the

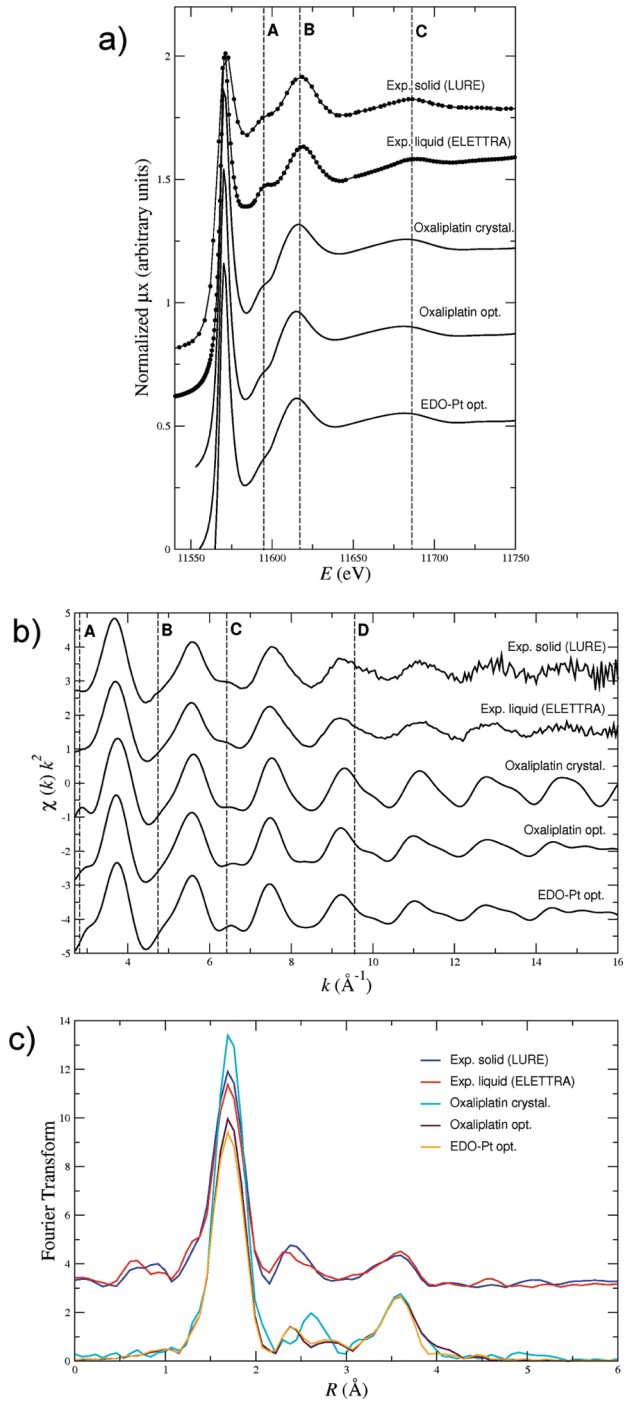

Figure 2. Comparison between experimental XANES (a) and EXAFS (b, c) spectra of solid and liquid samples of oxaliplatin, and theoretical spectra computed for the crystallographic structure of oxaliplatin and the gas-phase optimized oxaliplatin and EDO−Pt structures.

computed XANES is similar to that of the experimental liquid (ELETTRA) spectrum, which was recorded with a higher energy resolution in the edge region than the solid (LURE) one. The main difference concerns feature A, which is more defined in the experimental spectra than in the theoretical ones. However, this feature is almost identical for the three theoretical spectra, referred to as oxaliplatin crystal, oxaliplatin opt., and EDO−Pt opt. It can then be concluded that the contribution from the outer carbon atoms of the cyclohexane ring in the XANES spectrum is negligible.

When one examines the EXAFS spectra plotted in Figure 2 a noticeable overall similarity is found between all of them. The characteristic features of the experimental solid (LURE) and liquid (ELETTRA) spectra are well reproduced by the three theoretical spectra. The main differences are found for feature A, in the region of low-k values, which is difficult to modelize due to the importance of multiple scattering effects. In R-space the main difference observed when the five spectra are compared concerns the second peak (between 2.2 and 2.9 Å), which has been previously assigned to the Pt−C signal.[9] As mentioned in previous works[37] by some of the authors, the structural planarity and rigidity of oxaliplatin, especially in its oxalate part, lead to intricate contributions of a large number of scattering paths in the EXAFS function. Under such conditions slight variations in the structure may induce significant changes in the spectrum due to interference phenomena. Thus, if the three structural models considered in Figure 2 are closely examined, some differences among them appear concerning the Pt−C distances. The crystallographic structure is quite asymmetric, with four distinct Pt−C distances (2.71, 2.84, 2.87, 2.92 Å),[33] whereas the quantum mechanically optimized structures present only two different distances (two C at 2.81 Å and two C at 2.94 Å for EDO−Pt and two C at 2.82 Å and two C at 2.95 Å for oxaliplatin). An analysis of the partial contribution to the EXAFS by the scattering paths involving these carbon atoms showed how this small structural difference is enough to explain the change observed in the shape of the FT second peak when passing from oxaliplatin crystal to the two quantum mechanically optimized structures. It is worth noting that while such an asymmetry in the crystallographic structure may be explained in terms of packing effects, there is no reason for such a structural distortion to be observed in the liquid phase. As a matter of fact, a similar variation of the second peak of the FT is found when the two experimental spectra corresponding to the solid and the liquid samples are compared (red vs blue lines in Figure 2).

It is worth noticing that in k-space the three theoretical spectra are more structured than the experimental solid (LURE) and liquid (ELETTRA) spectra, particularly at high k-values. The theoretical EXAFS spectra were calculated without inclusion of any Debye−Waller factors. Therefore, the implicit static and dynamical disorder is not taken into account for these spectra, and the contributions of large distance scattering paths are overestimated. At the same time, the theoretical spectra computed for the two optimized models (oxaliplatin opt. and EDO−Pt opt.) are more structured than the one obtained for oxaliplatin crystal. This difference can be understood in terms of the higher asymmetry present in the crystallographic structure, which leads to destructive interference phenomena, as discussed above.

Finally, the spectra calculated for the optimized oxaliplatin and EDO−Pt structures are almost identical. We can thus conclude that the contribution from the outer carbon atoms of the cyclohexane ring is negligible for the EXAFS part as well. These results on XANES and EXAFS support, from a spectroscopical point of view, the use of EDO−Pt as a good model for oxaliplatin. The presence or absence of the cyclohexane ring does not generate any relevant features in the XAS spectra of oxaliplatin, and from the next section to the rest of the paper we will consider theoretical spectra obtained for EDO−Pt as a mimic for oxaliplatin.

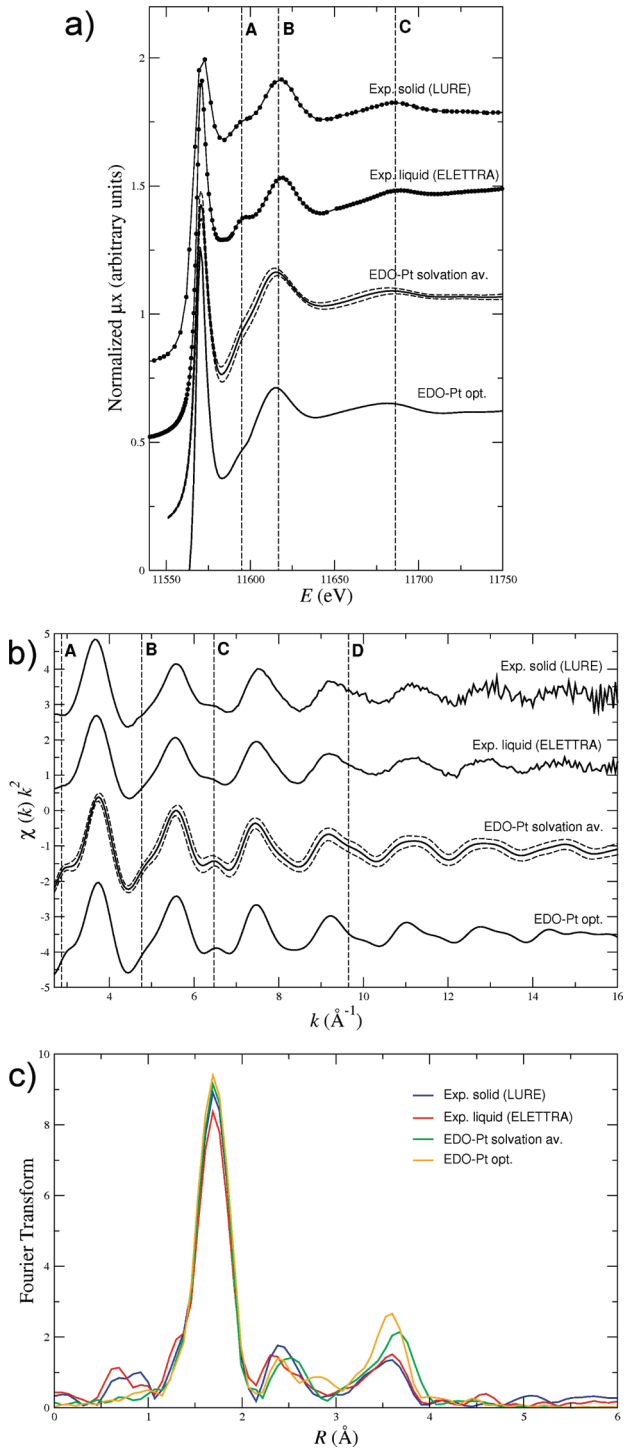

Figure 3. Theoretical XANES (a) and EXAFS (b, c) spectra of EDO−Pt obtained from a single quantum mechanically optimized structure (EDO−Pt opt.) and from the trajectory of a CP-MD simulation (EDO−Pt solvation av.) compared with experimental spectra of solid and liquid samples of oxaliplatin.

3.2. Analysis of Experimental Spectra by Means of Theoretical Spectra. The theoretical XANES and EXAFS spectra computed from the trajectory of the CP-MD simulation of EDO−Pt in aqueous solution (referred to as EDO-PT solvation av.) are plotted in Figure 3, together with the experimental XAS spectra recorded for the liquid and solid samples of oxaliplatin. The theoretical spectra computed for the quantum-mechanically optimized structure of EDO−Pt in gas phase is also included for the sake of comparison.

The theoretical EDO−Pt solvation av. and EDO−Pt opt. XANES spectra (Figure 3a) are almost identical. Both of them reproduce quite well the relative positions of the white line and the three features in the experimental spectra, although the hump labeled as feature A is more subtle in the theoretical spectra. The intensity of the white line in the computed XANES is similar to that of the experimental liquid ELETTRA spectrum. For the EXAFS part (Figure 3b) both the EDO−Pt opt. and EDO−Pt solvation av. theoretical spectra compare very well with the experimental ones, although the oscillations for k-values greater than 10 $Å^{-1}$ are better reproduced in the average spectrum obtained from the CP-MD trajectory (EDO−Pt solvation av.). As discussed in section 3.1, all theoretical signals calculated on the basis of a unique structure, without taking into account the structural disorder by means of the inclusion of Debye−Waller factors, overestimate the scattering signal beyond the first coordination sphere. This explains the supplementary structures observed in EDO−Pt opt. In the case of EDO−Pt solvation av., the structural disorder is implicitly taken into account when the average spectrum is obtained from a series of N structures from the conformational space. This leads to a better agreement with the experimental spectra. A good accordance is also observed in real space (see Figure 3c). It is worth noting that the peak intensity is greater in the EDO−Pt opt. spectrum due to the absence of any Debye−Waller factors in its computation.

Once we have shown that the theoretical spectra reproduce the experimental XANES and EXAFS remarkably well, it is illustrative to assess the influence of using a set of N snapshots instead of a single average structure to compute the spectra. That is how the structural fluctuations of the system, which are described along the MD trajectory by the N individual structures that compose the set, determines the average signal $\overline{\chi(k)}$. To this aim, at each k-value one can compute the mean standard deviation (MSD, σ_χ) associated with the average $\overline{\chi(k)}$ computed from the set of N structures (see eq 1):

$$\sigma_{\chi(k)} = \left[\frac{1}{N}\sum_{M=1}^{N}(\chi_M(k) - \overline{\chi(k)})^2\right]^{1/2} \quad (4)$$

Thus, the uncertainty ascribed to each k point of the spectrum can be obtained for a chosen degree of confidence $n\sigma_\chi$. We have computed such MSD for both the XANES and EXAFS theoretical average spectra of oxaliplatin in solution, and for each case it is plotted as two dashed lines defining a corridor of $2\sigma_\chi$ that encloses the average spectrum with a 95% degree of confidence (see Figure 3a,b). The thinness of both the EXAFS and XANES corridors indicates that the EDO−Pt complex behaves as a quite rigid structure in solution, as already concluded from our previous CP-MD results.[17] A close examination of the shape of the corridors suggests that in general the features in the average spectra are dumped if the MSD is considered.

3.3. Analysis of Contributions to the EXAFS Spectrum. In this section we aim to establish a correlation between the main features observed in the EXAFS spectrum (labeled A−D) and different structural motifs in oxaliplatin or, more precisely, in its model molecule EDO−Pt. To this purpose we have applied several cutoff criteria onto the CP-MD snapshots, which allowed the selection of distinct numbers of coordination shells around Pt to be included in the computation of the average $\overline{\chi(k)}$ (see Figure 1). Following this procedure, we obtained three different average EXAFS spectra corresponding to the contributions of

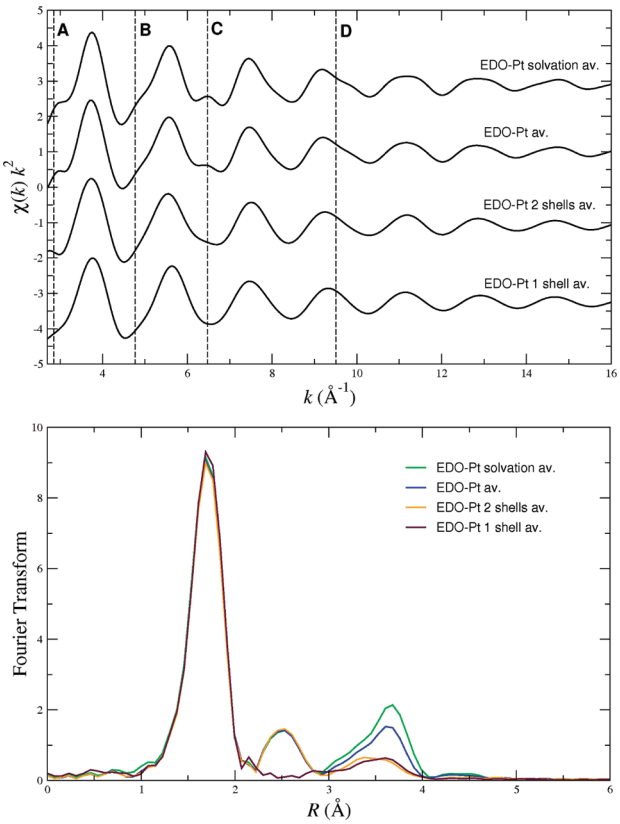

Figure 4. Decomposition of the average EXAFS spectrum of EDO−Pt in solution, as obtained from the CP-MD trajectory, into the contributions coming from different coordination shells around Pt.

one single coordination shell around Pt, two coordination shells, and the complete EDO−Pt complex. The resulting spectra are plotted in Figure 4 along with the EDO−Pt solvation av. spectrum presented in section 3.2, which includes solvent water molecules within a cutoff radius of 8 Å around the Pt center.

The spectrum labeled as EDO−Pt 1 shell av. includes only the contributions coming from the first coordination shell of atoms around Pt (i.e., the two N atoms and the two O atoms in the first shell, single and multiple scattering, see Figure 1). It is a rather simple wave. When a second shell of atoms is considered in the calculation (EDO−Pt 2 shells av.), feature A appears and the wave is slightly distorted in the regions of the other features. Further inclusion of the outer oxygen atoms from the oxalate ligand (EDO−Pt av. in Figure 4) defines the characteristic feature C and reinforces the change of slope associated to feature D.

Finally, the spectrum labeled EDO−Pt solvation av. takes into account the solvent contributions to the spectrum, which causes secondary changes in the shape of the EXAFS, namely, a slight change of slope associated with feature B and the enhancing of features C and D. Therefore, the complexity of the EXAFS signal is mainly originated by the structure of the EDO−Pt compound itself, and the solvent effects only introduce minor changes in *k*-space. On the basis of our previous analysis of the solvation structure of oxaliplatin by CP-MD simulations, we can expect the solvent effects to come from the contribution of water molecules that coordinate the inner oxygen atoms of the oxalate ligand (oxygen atoms in the first coordination shell of Pt) and the amine groups and water molecules that interact with the metal center in the axial region (see Figure 5). For both types of solvating water molecules, the average metal−oxygen distance is around 4.1 Å (for a detailed discussion of the

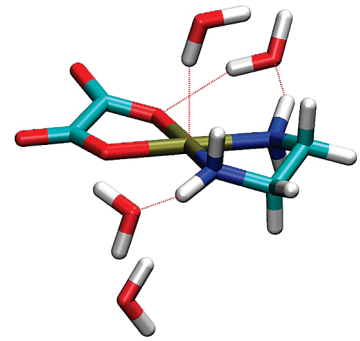

Figure 5. Representative configuration of the closest solvation pattern of EDO−Pt in solution, as described by ref 17. The oxygen atoms of water molecules are within a cutoff distance of 4.2 Å to the metal atom.

hydration pattern of oxaliplatin, see Figure 4 and Figure 6 in ref 17). Therefore, we can expect their backscattering effect on the EXAFS function to be similar to that of the outer oxygen atoms in the oxalate ligand, which are mainly responsible for features B and D, as discussed above. However, due to their dynamic behavior, the contribution of the solvating water molecules to the EXAFS spectrum is much more diffuse and their effect on the final signal is small.

This analysis is reinforced by observation of the nonphase-corrected Fourier transforms of these partial EXAFS spectra, plotted in Figure 4. The EDO−Pt 1 shell av. spectrum shows a well-defined peak around 1.7 Å in real space, corresponding to the average distance from Pt to atoms in its first coordination shell ($R_{Pt-O} = R_{Pt-N} = 2.04$ Å) as described in the MD simulation.[17] We also observe a minor component between 3 and 4 Å due to scattering through the platinum center, but almost no contribution of triangular multiple scattering paths, which should appear in the region between 2 and 3 Å. The bidentate nature of the two ligands in EDO−Pt generates angles of 84° and 96° in the first coordination shell of Pt. This distortion is sufficient to induce destructive interferences between the different triangular multiple scattering paths. In contrast, in structures such as $[Pt(H_2O)_4]^{2+}$, the highly symmetric square planar arrangement around platinum would lead to constructive interferences between the different triangular scattering paths.

When two shells of atoms around Pt are considered (labeled EDO−Pt 2 shells av.), a peak appears centered at 2.5 Å corresponding to the Pt−C single scattering paths, to be compared with the average Pt−C distance observed in the MD simulation ($R_{Pt-C} = 2.82$ Å). The inclusion of the outer oxygen atoms of the oxalate ligand in the calculation of the theoretical EXAFS spectrum induces a large increase of the third peak around 3.7 Å due to single and multiple scattering in the Pt−C−O part of the oxalate ligand. As already discussed in the analysis of the k^2-weighted EXAFS function, the scattering contributions of the solvent molecules appear at distances similar to those corresponding to scattering by the outer oxygen atoms in oxalate. Therefore, the peak at 3.7 Å is reinforced and the solvent effects to the EXAFS spectrum of EDO−Pt is clearly visible in real space.

It is worth emphasizing that the only difference between the sets of structures used to generate the EDO−Pt av. and EDO−Pt solvation av. spectra is the inclusion of solvent molecules in the latter. This procedure to obtain theoretical EXAFS spectra allows the unambiguous recognition of solvent effects in both the k^2-weighted and nonshifted Fourier transform spectra.

3.4. Fits of the EXAFS Spectra. In order to estimate the methodological error associated with the standard fitting pro-

TABLE 1: Parameters Obtained in the Best Fits of the Theoretical and Experimental EXAFS Signal[a]

parameter	EDO−Pt	EDO−Pt solv	ELETTRA	LURE	CP-MD	crystal
$R_{Pt-N/O}$	2.02(1)	2.02(1)	2.00(1)	1.99(1)	2.05(5)	2.04(2)
$R_{Pt-C_{ox}}$	2.76(3)	2.76(3)	2.74(4)	2.73(5)	2.83(5)	2.77(7)
$R_{Pt-C_{ed}}$	2.86(3)	2.86(3)	2.84(4)	2.83(5)	2.93(6)	2.90(3)
$R_{Pt-C-O_{II}}$	3.98(3)	3.98(2)	3.96(3)	3.94(4)	4.05(8)	4.00(2)
$R_{Pt-N-Pt-O}$	4.08(3)	4.08(2)	4.06(3)	4.04(4)	4.09(7)	4.07(2)
$\sigma_1^2 \times 10^4$	29(4)	29(4)	35(6)	33(7)		
$\sigma_2^2 \times 10^4$	78(25)	64(23)	70(30)	79(44)		
QF	2.72	3.20	3.22	1.72		

[a] EDO−Pt corresponds to the EDO−Pt av. spectrum, EDO−Pt solv to EDO−Pt solvation av., ELETTRA to liquid ELETTRA and LURE to solid LURE spectra. All distances are expressed in Å and the σ^2 values in Å^2. For a reference we include the average distances obtained from the CP-MD simulation of EDO−Pt (CP-MD) and from the crystallographic structure (crystal). $R_{Pt-C_{ed}}$ is constrained to $R_{Pt-C_{ox}} + 0.1$ Å, and $R_{Pt-N-Pt-O}$ to $R_{Pt-C-O_{II}} + 0.1$ Å. $R_{Pt-C-O_{II}}$ represents the three oxalate contributions: $Pt-O_{II}$, $Pt-C_{ox}-O_{II}$ and $Pt-C_{ox}-O_{II}-C_{ox}$.

cedure of the EXAFS spectra of oxaliplatin, we fitted under the same conditions both experimental spectra (solid LURE and liquid ELETTRA) and theoretical average spectra obtained from the CP-MD simulation (EDO−Pt av. and EDO−Pt solvation av.) One should note that, despite the low concentration in oxaliplatin, the high quality of the registered liquid ELETTRA spectrum allows us to perform an analysis on a much larger *k*-range than in the previous paper dealing with the spectrum of oxaliplatin in solution.[8]

A seven-shell model was used to describe the structure of EDO−Pt, including single scattering by the first neighbors (four Pt−N/O), single scattering by the four carbon atoms (two $Pt-C_{ox}$, two $Pt-C_{ed}$), single and multiple scattering signal due to the $Pt-C_{ox}-O_{II}$ part of the oxalate ligand (two $Pt-O_{II}$, four $Pt-C_{ox}-O_{II}$, two $Pt-C_{ox}-O_{II}-C_{ox}$), and multiple scattering through the platinum atom (four Pt−N−Pt−O; the Pt−N−O paths proved to be much less intense). As a high degree of correlation was observed between the different parameters, the feasibly highest number of constraints was imposed during the fitting procedure. The energy shift was fixed at 14 eV. The best fits were obtained when introducing 0.1 Å shifts between the two Pt−C contributions, on one hand, and between the three oxalate contributions ($Pt-O_{II}$, $Pt-C_{ox}-O_{II}$, $Pt-C_{ox}-O_{II}-C_{ox}$) and the multiple scattering paths through the platinum center, on the other hand. Therefore, we fitted only three distances (first shell Pt−N/O, second shell Pt−C, and a unique distance for paths contributing to the third peak in the FT, which may be considered as a reasonable approach if one realizes that the Pt−C−O bond is about 165°, sufficiently close to 180°) and two Debye−Waller factors (σ_1^2 for the single scattering related to the first coordination sphere and σ_2^2 for all other contributions). This seven-shell model does not include any contributions from the solvent. The results of the fits of the four EXAFS spectra are presented in Table 1, along with reference data from the CP-MD simulation and the crystallographic structure. All spectra are fitted with reasonable parameters and all distances obtained from the fits are close to the structural ones. All quality factors are greater than 1 but nevertheless close to 1, meaning that systematic errors predominate for all spectra.

It is worth noting that while the crystallographic structure serves as reference data for the fitting of experimental data, whether the experimental sample is in the same phase (crystalline solid) or not (powder for pharmaceutical use or liquid solution in our case), the distances obtained from direct analysis of the CP-MD simulation constitute the current values of the structural parameters discussed in Table 1 for the two theoretical spectra. Therefore, the comparison between the data obtained from fitting the EDO−Pt av. or EDO−Pt solvation av. spectra with the CP-MD structural data provides an immediate estimation of the errors introduced by the methodology employed in the fitting procedure. We observe that our seven-shell model induces a small overall underestimation of the radial structural distances, this underestimation being larger as the coordination shell is further away from Pt. Thus, the distances within the first coordination shell (Pt−N/O) are 0.03 Å too short, and the error in the second and third shells (Pt−C and Pt−O) is about 0.07 Å. In consequence, at least the same error bars should be considered when dealing with the distances fitted for liquid ELETTRA and solid LURE spectra, even though the precision seems to be higher from the fit analysis. Under these conditions, the four EXAFS spectra yield indistinguishable structural distances.

All fitted distances obtained from EDO−Pt av. and EDO−Pt solvation av. are identical, as expected, since the only difference between these two spectra is the absence or presence of solvent contributions. The Debye−Waller factor for single scattering within the first coordination shell (σ_1^2) is also equivalent for the two theoretical spectra. However, differences appear in the σ_2^2 factors, which collect contributions of other coordination shells and multiple scattering paths. The lower σ_2^2 value obtained for EDO−Pt solvation av. and the quality factors suggest that the fit of EDO−Pt solvation av. may be lacking the consideration of scattering paths including solvent molecules. Figure 6 shows that for both experimental and theoretical spectra, the seven-shell model correctly fits the complete EXAFS spectrum. Only for EDO−Pt solvation av. the seven-shell model does not completely reproduce the third peak in the Fourier transform.

The question has arisen whether it is possible or not to detect the water molecules of solvation by means of a standard analysis of the EXAFS spectrum. The comparison of the FT of the theoretical EDO−Pt av. and EDO−Pt solvation av. spectra (Figure 4) already suggested that the main contribution from the solvent appears around 4 Å from the metal center. The difference spectrum between the two theoretical spectra in *k*- and *R*-spaces is shown in Figure 7. The FT of this difference shows a well-defined peak compatible with such a distance. A reasonable fitting of this peak is achieved using a model containing a single shell of three water molecules around Pt. Even if it appears difficult to obtain very convincing amplitude parameters, we observe a very stable distance of the water molecules to platinum of 4.14 Å, in good agreement with the mean Pt−O distance observed in the CP-MD simulation (around 4.1 Å).[17]

In order to assess this result and to try an improvement of the fits of the EXAFS spectra in liquid phase, one shell of water molecules has been added to the previous seven-shell model. A new fitting has been carried out including as new parameters the number of water molecules and their mean distance to Pt

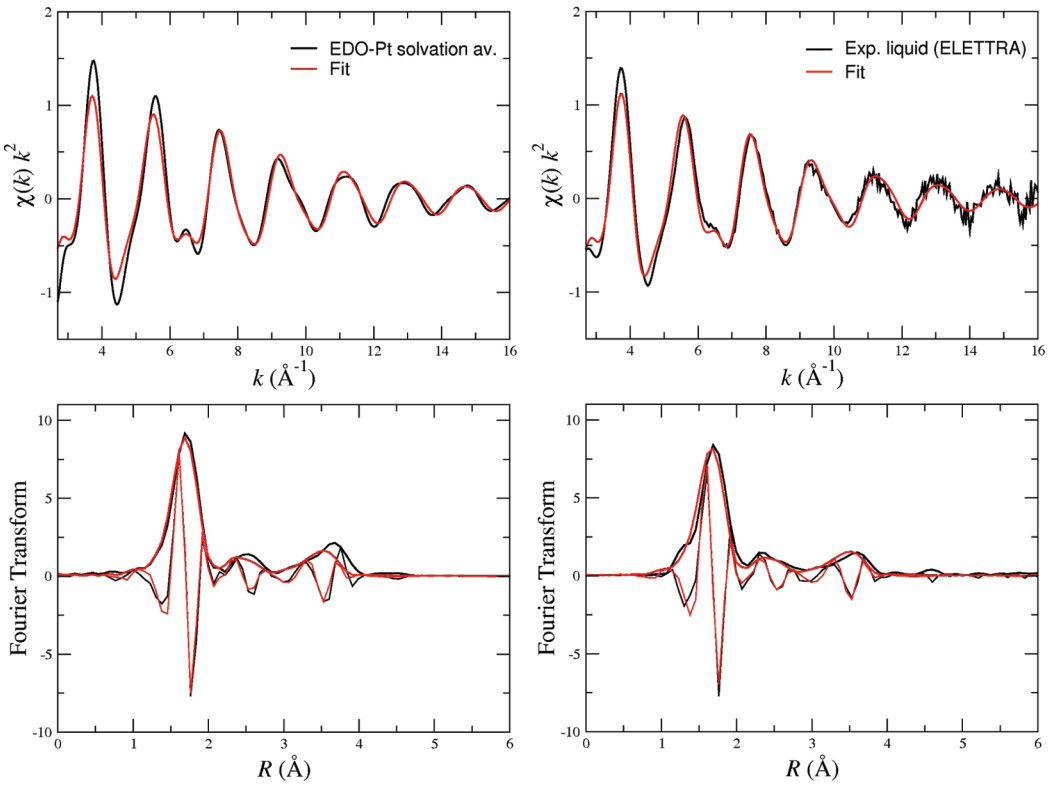

Figure 6. Fits to the average EXAFS spectra of EDO−Pt including solvation and to the experimental ELETTRA spectrum (liquid sample).

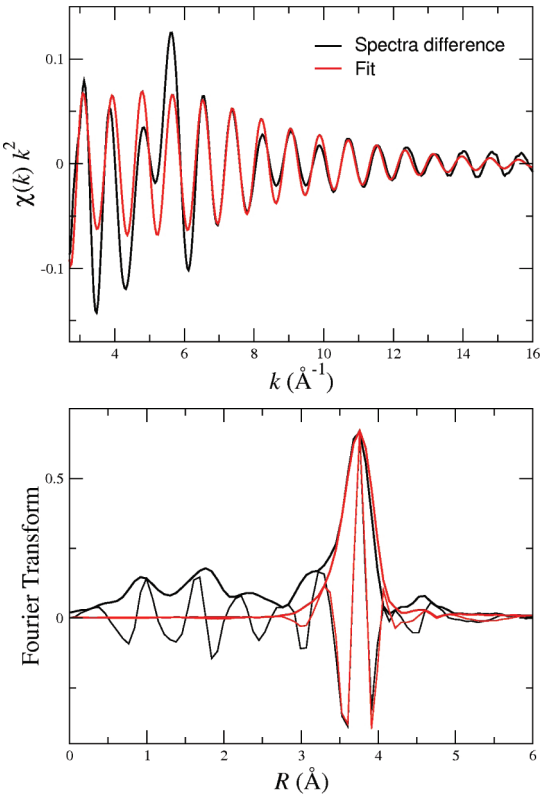

Figure 7. Fit to the difference between EDO−Pt solvation av. and EDO−Pt av. spectra. The resulting parameters are $N_{H_2O} = 3(2)$; $\sigma_w^2 = 56(57) \times 10^{-4}$ Å^2; $R_{H_2O} = 4.14(3)$ Å; residual = 0.33; QF = 0.08.

and using two different constraints on the corresponding Debye−Waller factors ($\sigma_w^2 = \sigma_2^2$ or $\sigma_w^2 = 2\sigma_2^2$). Such fits were performed for both EDO−Pt solvation av. and EDO−Pt av. theoretical spectra, in order to check that this additive shell does not compensate systematic errors. The results of the fits are gathered in Table 2, along with the results of the fits without including the solvent ("no H_2O" column). The number of water molecules and their structural distance, obtained from the fit of the EDO−Pt solvation av. spectrum, are coherent with the values obtained by fitting the spectra difference. They do not depend on the constraint on the Debye−Waller factor associated with the solvent contribution. In contrast, the fits of EDO−Pt av. result in about zero water molecules, as expected.

In *k*-space, the value of $\Delta\chi^2$ does not change for EDO−Pt av. when the shell of water molecules is included in the fit. Contrarily, the value of $\Delta\chi^2$ decreases in the case of EDO−Pt solvation av. but not sufficiently to compensate for the introduction of additional parameters in the fit. The quality factor is not significantly affected by the consideration of solvent effects in the fit, neither for EDO−Pt av. nor for EDO−Pt solvation av. In contrast, in *R*-space there is an appreciable reduction in the values of the residuals beyond the first peak in the FT when water molecules are considered in the fit of EDO−Pt solvation av., meaning that the fit is significantly improved: the addition of water molecules improves the residual factor, in the range 2.15−4.07 Å, from 25% to 12%−16% for EDO−Pt solvation av., while the same factor remains between 15% and 17% for EDO−Pt av. with almost no water being found. However, the large error bars on the number of water molecules and the difficulty to obtain convincing amplitude parameters make it hazardous to determine the solvent effects with confidence. This suggests that the solvation structure of EDO−Pt may be determined by EXAFS analysis, but more refined fitting procedures are mandatory to achieve this goal, together with a new set of experimental data for oxaliplatin in solid and solution with a high signal/noise ratio.

4. Concluding Remarks

Theoretical EXAFS and XANES spectra of the L_{III}-edge of Pt for the EDO−Pt model of oxaliplatin have been obtained by

TABLE 2: Parameters of the Fits of the Theoretical EDO−Pt Av. and EDO−Pt Solvation Av. Spectra without Including Water (no H_2O) or Including Solvent Water Molecules, Using Different Constraints on the Debye−Waller Factors[a]

	EDO−Pt solvation av.			EDO−Pt av.		
parameter	no H_2O	$\sigma_w^2 = \sigma_2^2$	$\sigma_w^2 = 2\sigma_2^2$	no H_2O	$\sigma_w^2 = \sigma_2^2$	$\sigma_w^2 = 2\sigma_2^2$
R_{Pt-NO}	2.02(1)	2.02(1)	2.02(1)	2.02(1)	2.02(1)	2.02(1)
$R_{Pt-C_{ox}}$	2.76(3)	2.75(4)	2.75(4)	2.76(3)	2.76(3)	2.76(3)
$R_{Pt-C_{ed}}$	2.86(3)	2.85(4)	2.85(4)	2.86(3)	2.86(3)	2.86(3)
$R_{Pt-C-O_{II}}$	3.98(2)	3.98(3)	3.98(3)	3.98(3)	3.98(3)	3.98(3)
$R_{Pt-N-Pt-O}$	4.08(2)	4.08(3)	4.09(3)	4.08(3)	4.08(3)	4.08(3)
N_{O_w}		4(3)	4(3)		1(1)	0(9)
R_{O_w}		4.15(5)	4.15(7)		4.16(22)	4.13(22)
$\sigma_1^2 \times 10^4$	29(4)	29(4)	29(4)	29(4)	29(4)	29(4)
$\sigma_2^2 \times 10^4$	64(23)	71(27)	64(23)	78(25)	80(31)	79(28)
$\sigma_w^2 \times 10^4$		71(27)	128(46)		80(31)	158(56)
$\Delta\chi^2$	96.11	88.70	91.78	81.72	81.72	81.72
QF	3.20	3.17	3.28	2.72	2.91	2.92
$\rho_{FT} \times 10^2$	25.23	12.23	15.92	17.26	15.32	17.32

[a] The number of water molecules is fitted when water is included. ρ_{FT} is the residual in *R*-space, calculated on the signal beyond the first coordination sphere (2.15−4.07 Å) of the Fourier transform.

using a high number of structural configurations provided by a previous CP-MD simulation of this compound in bulk water[17] and the FEFF code for ab initio multiple scattering calculations of the X-ray absorption spectrum. The agreement between the resulting theoretical and the available experimental spectra is remarkably good, providing a validation of both our ab initio MD representation of the complex and the theoretical tools used to compute the XAS spectra, and supports the use of EDO−Pt to mimic oxaliplatin in a spectroscopical framework.

The combination of theoretical and experimental XAS techniques provides the possibility to extract refined information on the complex under study. In particular, the computation of EXAFS spectra using different numbers of coordination shells around the absorbing atom allows the assignment of spectral features to particular structural motifs in the complex. This type of analysis, only possible from the theoretical point of view, allows the understanding of the EXAFS spectrum not only in *R*-space but already in *k*-space. Within our methodology, the outer oxygen atoms of the oxalate ligand can be undoubtedly detected in the EXAFS spectrum of oxaliplatin. This result supports the conclusions derived in a previous paper by some of us,[9] where the contribution of the scattering paths implying these O_{II} atoms were identified in the Fourier transform of the EXAFS spectrum. Furthermore, the assignment of the oxalate ligand to a specific feature in the EXAFS *k*-spectrum derives in a very interesting potential application of this oxalate *signature* to the determination of derivatives of oxaliplatin. During its physiological activity, oxaliplatin is decomposed and one or two of its coordination ligands can be substituted by different biological nucleophiles. If the mechanism of action of oxaliplatin is close to that of cisplatin, it should lead to the formation of aquo−platinum(II) complexes in the cell. Since the presence or absence of the oxalate ligand can be experimentally evaluated from the EXAFS spectrum, this opens the door to the study of ligand exchange processes by means of XAS-related techniques such as quick EXAFS or dispersive XAFS. Reversely, the cyclohexane ring present in the diamine ligand of oxaliplatin is found not to generate by itself any feature in the EXAFS nor the XANES spectra of oxaliplatin, which implies that the related scattering paths do not represent an important contribution to the total XAS spectra of the complex. Instead, only the carbon atoms of the ring that are directly bonded to the amino groups are involved in the scattering paths contributing to the EXAFS function.

The comparison of the structural data obtained from the fits of the MD-based theoretical EXAFS spectra with the data derived from direct analysis of the MD trajectory used to produce the same theoretical spectra has led to the evaluation of the methodological error associated with the fitting procedure. As a conclusion, the maximum possible precision on the distances for scattering beyond the second coordination shell (±0.04 Å) is about half the precision characterizing the determination of the first shell around Pt (±0.02 Å). However, given the high structural rigidity of oxaliplatin, this error is small enough to permit a high degree of confidence in the structural determination of the oxalate ligand, whose distances belong to a range usually hardly accessible by EXAFS analysis of liquid samples.

The hydration structure around EDO−Pt has been qualitatively detected by decomposing the theoretical EXAFS spectrum of the complex into the contributions coming from the complex itself and from the solvent, the latter being understood in terms of water molecules that coordinate the inner oxygen atoms of the oxalate and the amine groups in the first coordination sphere of Pt. The partial EXAFS signal attributed to the solvent effect, although of very small magnitude, has been fitted to a shell of water molecules. Furthermore, the solvent contribution has been extracted from a fit of the theoretical EXAFS spectrum of EDO−Pt in solution, and the results obtained in this fit are coherent with the rest of information available. However, the intrinsic weakness and lability of the solvation shell around EDO−Pt prevents its sufficiently accurate determination by means of a standard EXAFS fit. A more refined analysis procedure of the EXAFS spectrum is thus mandatory to achieve the determination of the solvation structure of EDO−Pt or oxaliplatin in liquid water. It would also be desirable to obtain access to experimental spectra of solid and liquid samples of oxaliplatin recorded under the same experimental setup with a high signal-to-noise ratio, which would allow the study of the EXAFS part in a wider *k*-range. Work is in progress for the exploration of both possibilities.

When dealing with theoretical EXAFS spectra derived from MD trajectories, the role of the Debye−Waller factor is played by the average over a large number of individual spectra contributing in a statistical manner to the observed EXAFS spectrum. An intimate consequence of this microscopical construction of the EXAFS signal is that no model structure has to be defined in order to analyze it. However, if one

envisages to perform an EXAFS analysis within the standard procedure by using a model and fitting to the EXAFS signal, the Debye−Waller factors do not need to be fitted, but they can rather be obtained from the trajectory of the molecular dynamics simulation. Such a procedure, which would dramatically decrease the number of variables in the fit, is a potentially powerful fitting strategy which must be carefully explored in the future.

The methodology here employed goes beyond the rather common theoretical−experimental comparison and the mutual support found when both sets of results are close. The inclusion of microscopic structural and dynamic information within the global analysis of the EXAFS and XANES data reveals a powerful synergy that constitutes one the most promising ways to widen the capabilities of X-ray absorption techniques in solution.

Acknowledgment. We would like to thank Prof. Gilberto Vlaic, Dr. Luca Olivi, Dr. Jacques Moscovici, and Pr. Simone Bénazeth for data collection at LURE and ELETTRA. We would also like to thank Prof. Alain Michalowicz for useful discussions. The European Community Research Infrastructure Action under the FP6 Structuring the European Research Area Program (through the Integrated Infrastructure Initiative Integrating Activity on Synchrotron and Free Electron Laser Science) and the Spanish Ministerio de Ciencia e Innovación (CTQ2008-05277) are gratefully acknowledged for financial support. E.C.B. acknowledges Junta de Andalucía for a postdoctoral fellowship (P06-FQM-01484).

References and Notes

(1) Graham, J.; Muhsin, M.; Kirkpatrick, P. *Nat. Rev. Drug Discovery* **2004**, *3*, 11–12.

(2) Avendaño, C.; Menéndez, J. C. *Medical Chemistry of Anticancer Drugs*; Elsevier: Amsterdam, 2008.

(3) Voland, C.; Bord, A.; Péleraux, A.; Pénarier, G.; Carrière, D.; Galiègue, S.; Cvitkovic, E.; Jbilo, O.; Casellas, P. *Mol. Cancer Ther.* **2006**, *5*, 2149–2157.

(4) Fischel, J.; Rostagno, P.; Formento, P.; Dubreuil, A.; Etienne, M.; Milano, G. *Br. J. Cancer* **2001**, *84*, 579–585.

(5) Ho, Y. P.; An-Yeung, S.; To, K. *Med. Res. Rev.* **2003**, *23*, 633–655.

(6) Kelland, L. *Nat. Rev. Cancer.* **2007**, *7*, 573–584.

(7) Peacock, A. F. A.; Parsons, S.; Sadler, P. J. *J. Am. Chem. Soc.* **2007**, *129*, 3348–3357.

(8) Curis, E.; Provost, K.; Bouvet, D.; Nicolis, I.; Crauste-Manciet, S.; Brossard, D.; Bénazeth, S. *J. Synchrotron Radiat.* **2001**, *8*, 716–718.

(9) Bouvet, D.; Michalowicz, A.; Crauste-Manciet, S.; Curis, E.; Nicolis, I.; Olivi, L.; Vlaic, G.; Brossard, D.; Provost, K. *J. Synchrotron Radiat.* **2006**, *13*, 477–483.

(10) Filipponi, A.; D'Angelo, P.; Pavel, N. V.; Di Cicco, A. *Chem. Phys. Lett.* **1994**, *225*, 150.

(11) Palmer, B. J.; Pfund, D. M.; Fulton, J. L. *J. Phys. Chem.* **1996**, *100*, 13393.

(12) Campbell, L.; Rehr, J. J.; Schenter, G. K.; McCarthy, M. I.; Dixon, D. *J. Synchrotron Radiat.* **1999**, *6*, 310.

(13) Merkling, P. J.; Muñoz-Páez, A.; Martínez, J. M.; Pappalardo, R. R.; Sánchez Marcos, E. *Phys. Rev. B* **2001**, *64*, 012201.

(14) Merkling, P. J.; Muñoz-Páez, A.; Sánchez Marcos, E. *J. Am. Chem. Soc.* **2002**, *124*, 10911.

(15) Merkling, P. J.; Muñoz-Páez, A.; Pappalardo, R. R.; Sánchez Marcos, E. *Phys. Rev. B* **2001**, *64*, 092201.

(16) D'Angelo, P.; Roscioni, O.; Chillemi, G.; Longa, S. D.; Benfatto, M. *J. Am. Chem. Soc.* **2006**, *128*, 1853–1858.

(17) Beret, E. C.; Pappalardo, R. R.; Marx, D.; Sánchez Marcos, E. *ChemPhysChem* **2009**, *7*, 1044–1052.

(18) Car, R.; Parrinello, M. *Phys. Rev. Lett.* **1985**, *55*, 2471–2474.

(19) Marx, D.; Hutter, J. In *Modern Methods and Algorithms of Quantum Chemistry*; Grotendorst, J., Ed.; NIC FZ: Jülich, 2000, see www.theochem-.rub.de/go/cprev.html.

(20) Carrera, F.; Torrico, F.; Richens, D. T.; Muñoz-Páez, A.; Martínez, J. M.; Pappalardo, R. R.; Sánchez Marcos, E. *J. Phys. Chem. B* **2007**, *111*, 8223–8233.

(21) Perdew, J. P.; Burke, K.; Ernzerhof, M. *Phys. Rev. Lett.* **1996**, *77*, 3865.

(22) Andrae, D.; Haeussermann, U.; Dolg, M.; Stoll, H.; Preuss, H. *Theor. Chim. Acta* **1990**, *77*, 123.

(23) Dunning, T. H. J. *J. Chem. Phys.* **1989**, *90*, 1007.

(24) Ankoudinov, A. L.; Ravel, B.; Rehr, J. J.; Conradson, S. D. *Phys. Rev. B* **1998**, *58*, 7565–7576.

(25) Ankoudinov, A. L.; Bouldin, C. E.; Rehr, J. J.; Sims, J.; Hung, H. *Phys. Rev. B* **2002**, *65*, 1041071–11.

(26) Ankoudinov, A. L. Ph.D. thesis, University of Washington, 1996.

(27) Merkling, P.; Ayala, R.; Martínez, J. M.; Pappalardo, R. R.; Sánchez Marcos, E. *J. Chem. Phys.* **2003**, *119*, 6647–6654.

(28) Ayala, R.; Martínez, J. M.; Pappalardo, R. R.; Muñoz-Páez, A.; Sánchez Marcos, E. *Mol. Simul.* **2006**, *32*, 1035–1044.

(29) Teo, B. K. *Inorganic Chemistry Concepts. EXAFS: Basic Principles and Data Analysis*; Springer-Verlag: Berlin, 1986; Vol. 9.

(30) Koenigsberger, D. C.; Prins, R. *X-ray Absorption: Principles, Applications, Techniques of EXAFS, SEXAFS and XANES*; Wiley: New York, 1988.

(31) Lytle, F. W.; Sayers, D. E.; Stern, E. A. *Physica B* **1989**, *158*, 701–722.

(32) Michalowicz, A. Outils et méthodes pour l'analyse des spectres EXAFS, http://www.icmpe.cnrs.fr/spip.php?article578.

(33) Bruck, M. A.; Bau, R.; Noji, M.; Inagaki, K.; Kidani, Y. *Inorg. Chim. Acta* **1984**, *92*, 279–284.

(34) Provost, K.; Champloy, F.; Michalowicz, A. *J. Synchrotron Radiat.* **2001**, *8*, 1109–1112.

(35) IXS(2000), Error reporting recommendations: A report of the standards and criteria committee, http://www.i-x-s/org/OLD/subcommittee_reports/sc/.

(36) Vlaic, G.; Andreatta, D.; Cepparo, A.; Colavita, P. E.; Fonda, E.; Michalowicz, A. *J. Synchrotron Radiat.* **1999**, 225–227.

(37) Bouvet, D.; Michalowicz, A.; Crauste-Manciet, S.; Brossard, D.; Provost, K. *Inorg. Chem.* **2006**, *45*, 3393.

JP905415V